Electrochemical deposition of Cu-doped p-type iron oxide thin films

Satoshi Kobayashi[1] and Masaya Ichimura[2]

Department of Electrical and Mechanical Engineering, Nagoya Institute of Technology, Gokiso Showa, Nagoya 466-8555, Japan

E-mail: [1]cli13087@stn.nitech.ac.jp, [2]ichimura.masaya@nitech.ac.jp

Abstract

Fe_2O_3 and γ-FeOOH, major constituents of iron rust, are an n-type semiconductor with a bandgap of 2.0~2.6 eV. In this work, we deposited Cu-doped p-type iron oxide by electrochemical deposition method. p-type iron oxide is expected to be applied for photo-cathodes in electrochemistry and also for pn junction solar cells. The films were deposited from an aqueous solution containing $FeSO_4$ and $CuSO_4$ and annealed in air at 400ºC. The conduction type was converted into p-type when the ratio of copper to iron in the film was about 10% or more. Annealing in air improved film adhesion to the substrate and enhanced p-type conductivity.

Keywords: electrochemical deposition(ECD), iron oxide, p-type semiconductor, copper doping

1. Introduction

Iron oxide is a low cost and nontoxic material, and has been extensively studied as a magnetic material and a semiconductor in broad fields. Among various phases of iron oxides, hematite α-Fe_2O_3 is an n-type semiconductor with a bandgap of about 2 eV and considered to be promising for a photocatalyst (photo anode)[1]. Iron oxyhydroxide FeOOH has a purifying action for aqueous solutions[2],[3] and is also used as a precursor of hematite. γ-FeOOH is an n-type semiconductor with a band gap of 2.2 eV to 2.6 eV[4], and it has been fabricated by a spray method, hydrolysis of Fe ions[5-8] and electrochemical deposition (ECD)[4,9-12]. It is known that γ-FeOOH is thermally decomposed to γ-Fe_2O_3 at 200 ºC, and then converted to a more stable phase, α-Fe_2O_3 at 400 ºC[13].

It has been reported that the conduction type of iron oxide can be converted to p-type by doping of Cu, Zn, and Mg[14-17]. p-type iron oxide can be used for a photo cathode, and is expected to be able to realize self-driven water photolysis, combined with an n-type iron oxide photo anode[14-17]. In addition, low-cost solar cells may be fabricated based on pn homo-junction formed with p-type and n-type iron oxides. Thus p-type iron oxide is a potentially useful energy material.

In this work, we deposit Cu-doped p-type iron oxide by ECD. In the ECD method, the potential or current density is controlled with an external device, and thin films are deposited by the oxidation or reduction reaction at the substrate. ECD is suitable for fabricating large-area thin films because of the following advantages [18]; (i) The deposition does not need vacuum environment or high-temperature heater, and thus the equipment is simple and inexpensive. (ii) The film composition can be controlled by adjusting the solution composition and other deposition parameters. In this work, we fabricate thin films by potentiostatic (constant potential) ECD. In addition, we anneal the deposited films in air

22 (oxidizing) ambient. The annealing will modify crystallinity of the film. Moreover, it may reduce

23 concentration of oxygen-deficiency defects acting as a donor[19] and thus enhance p-type conductivity.

24 The results show that the films show p-type conduction with Cu to Fe ratio larger than about 10 %.

25

26 **2. Experimental methods**

27 For deposition, a three electrode cell was used with a platinum sheet and a Ag/AgCl electrode used

28 as the counter electrode (CE) and the reference electrode (RE), respectively. The working

29 electrode(WE) or substrate was an indium-tin-oxide (ITO) coated glass sheet of about 10 Ω/square

30 sheet resistance. A potentiostat/galvanostat HA-151B (Hokuto-Denko) and a function generator

31 HB-315 (Hokuto-Denko) were used in the deposition and cyclic voltammetry (CV) measurement. The

32 ITO substrate was washed with acetone for 5 min and deionized (DI) water for 5 min ultrasonically.

33 The deposition area was 1x1 cm^2.

34 The deposition solution for FeOOH[4] contained 50 mM iron sulfate (FeSO$_4$·7H$_2$O), and 100 mM

35 sodium sulfate (Na$_2$SO$_4$) as a supporting electrolyte. Different concentration of copper sulfate (CuSO$_4$)

36 (0.5, 1, 2.5, 5, 10 mM) was added to that solution as a doping agent. Approximately 50 mL of DI water

37 was used as a solvent. The solution temperature was adjusted to 15ºC by using a cool stirrer (SCINICS

38 CPS-300), and high purity oxygen gas (99.6 %) was blown into the solution for 10 min to saturate it

39 with oxygen. In the deposition, constant potential of -0.86 V was applied for 10 min, while the

40 solution was stirred at 300 rpm. The deposited thin films were annealed in air at 400ºC for 60 min

41 without setting the heating and cooling rate.

42 In the CV measurement, the potential was swept from 0 V to -1.5 V followed by -1.5 V to 0.5 V and

43 finally from 0.5 V to 0 V at a scan rate of 20 mV/s. Film thicknesses were measured via a profilometer

44 Surfcom-1400D (ACCRETECH-Tokyo Seimitsu). Compositional analysis was conducted by

45 JAMP-9500F field emission Auger microprobe (JEOL) at a prove voltage of 10 keV and a current of 1

46 $\times 10^{-8}$ A. Before the measurement, contaminants were removed from the thin-film surface by Ar ion

47 etching, whose rate was about 10 nm per min for SiO$_2$. Scanning electron microscopes (SEM) images

48 were also taken by JAMP-9500F. Raman spectra were analyzed by a laser Raman spectrophotometer

49 NRS-3300 (JASCO) using a 632.8 nm red laser as an excitation source. X-ray diffraction (XRD)

50 patterns were recorded with SmartLab X-ray diffractometer (Rigaku) using a CuKα radiation source.

51 Optical transmittance was measured in the range of 300 nm to 1500 nm wavelength using a V-570

52 UV/VIS/NIR double beam spectrophotometer (JASCO). Photoelectrochemical (PEC) measurement

53 was conducted using the same three-electrode cell as for the deposition and a Xenon lamp (100

54 mW/cm^2) in an aqueous electrolyte of 100 mM Na$_2$SO$_4$. The applied voltage was swept from 0 V to ±1

55 V at 5 mV/s, and the illumination was mechanically chopped (on and off) for each 5 seconds. The

56 conductivity type is judged by observing the photo-response of minority carriers of the sample. When

57 the negative photocurrent is dominantly observed under negative potentials, the conduction type is

58 judged p-type. If the positive photocurrent is dominant, the conduction type is judged n-type.

59 Electrochemical impedance measurement was conducted using LCR meter ZM2371 (NF) at a

60 frequency of 1 kHz and an amplitude of 10 mV in an aqueous electrolyte of 100 mM Na$_2$SO$_4$.

61

62 **3. Results and discussion**

63 Fig.1 shows CV for the FeOOH deposition solutions without $CuSO_4$ and with 0.5, 2.5 and 10 mM
64 $CuSO_4$ included. All the deposition solutions show anodic and cathodic peaks, and intensity of the
65 cathodic current is significantly different between the solutions during the initial scan from 0 V to -1.5
66 V. In the FeOOH deposition solution, almost no cathodic current flowed in a range from 0 V to -0.8 V,
67 and slight cathodic current flowed in a range from -0.8 V to -1.0 V, and then current increased more
68 steeply for potentials more negative than -1.0 V. The FeOOH film was deposited in the range from -0.8
69 V to -1.0 V, and metallic iron was also deposited at more negative potentials. In contrast, in the
70 deposition solutions including $CuSO_4$, small negative current flowed in a range from about 0 V to -0.8
71 V. The cathodic current intensity increased with $CuSO_4$ concentration, and only copper oxide was
72 deposited in this range. Mixed copper and iron oxides were deposited around -0.85 V for all the
73 solutions with $CuSO_4$. As for the FeOOH deposition solution, metallic iron was also deposited at
74 potentials more negative than -1.0 V. On the basis of the above observations, all the Cu-doped films
75 were deposited at -0.86 V. An anodic peak was observed around 0.2 V when $CuSO_4$ was added to the
76 solution. Since the peak was not observed for the solution without $CuSO_4$, the peak is attributed to
77 reactions involving Cu compounds. In previous works of ECD of copper oxide, an anodic peak in CV
78 was observed in a range of 0.15-0.22 V vs Ag/AgCl [20, 21]. The possible reaction would be
79 dissolution of copper oxide and/or oxidation of Cu_2O to CuO.
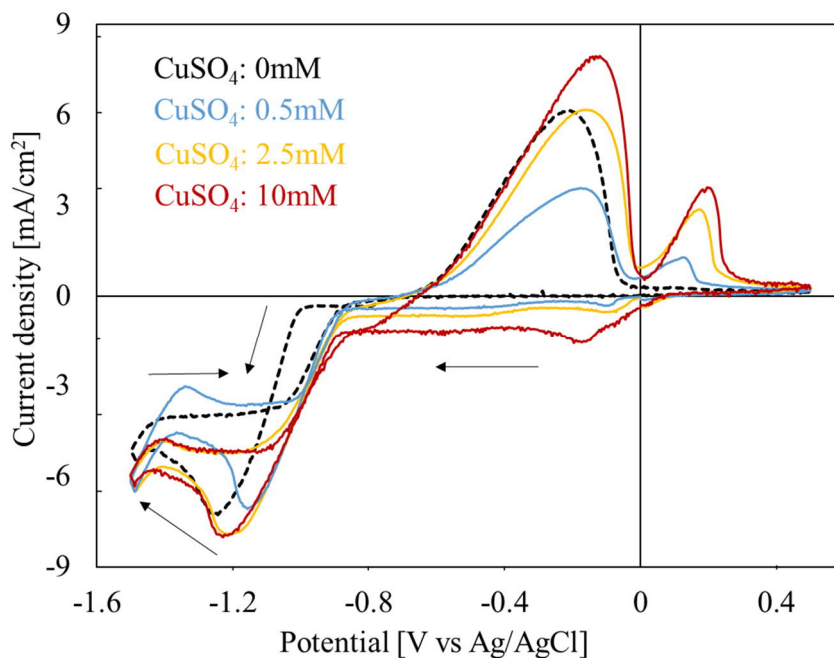
80
81 Fig.1 CV for the solutions without and with different $CuSO_4$ concentrations.

82
83 The color of the deposited films changed from yellow to darkened yellow as the concentration of
84 $CuSO_4$ increased. After the annealing, the color of the films changed to reddish brown. In the thickness
85 measurement, the thickness of the as-deposited films could not accurately be measured because the
86 thin films were scratched by the profiler probe. On the other hand, after the annealing, the films were
87 hard enough for the measurement, and the film thickness was measured to be approximately 0.2 - 0.7
88 μm for all the Cu-doped samples (the film thickness was not uniform within the sample).
89 Figs.2 (a) - (h) show the SEM images of the films deposited with different $CuSO_4$ concentrations

90　before and after the annealing. Difference in CuSO$_4$ concentration resulted in the surface morphology

91　of different grain sizes. Figs.2 (a) and (b) are the SEM image of the FeOOH film without Cu doping

92　before and after the annealing, respectively. With CuSO$_4$ concentration of 1 mM, the grains on the

93　surface grew larger than in Figs.2 (a) and (b). For CuSO$_4$ concentration of 2.5 mM, many fine grains

94　were deposited, as shown in Figs. 2 (e) and (f). In Fig.2 (g) and (h), it was observed that grains again

95　grew larger. After the annealing, for CuSO$_4$ concentration of 2.5 mM or less, the grains were observed

96　more clearly than before the annealing, i.e., the grains appeared to be more compactly aggregated.

97　This may be related to improved hardness of the film. For CuSO$_4$ concentration of 5 mM or more, no

98　significant change was seen after the annealing.

(a)

(b)

(c)

(d)

(e)

(f)
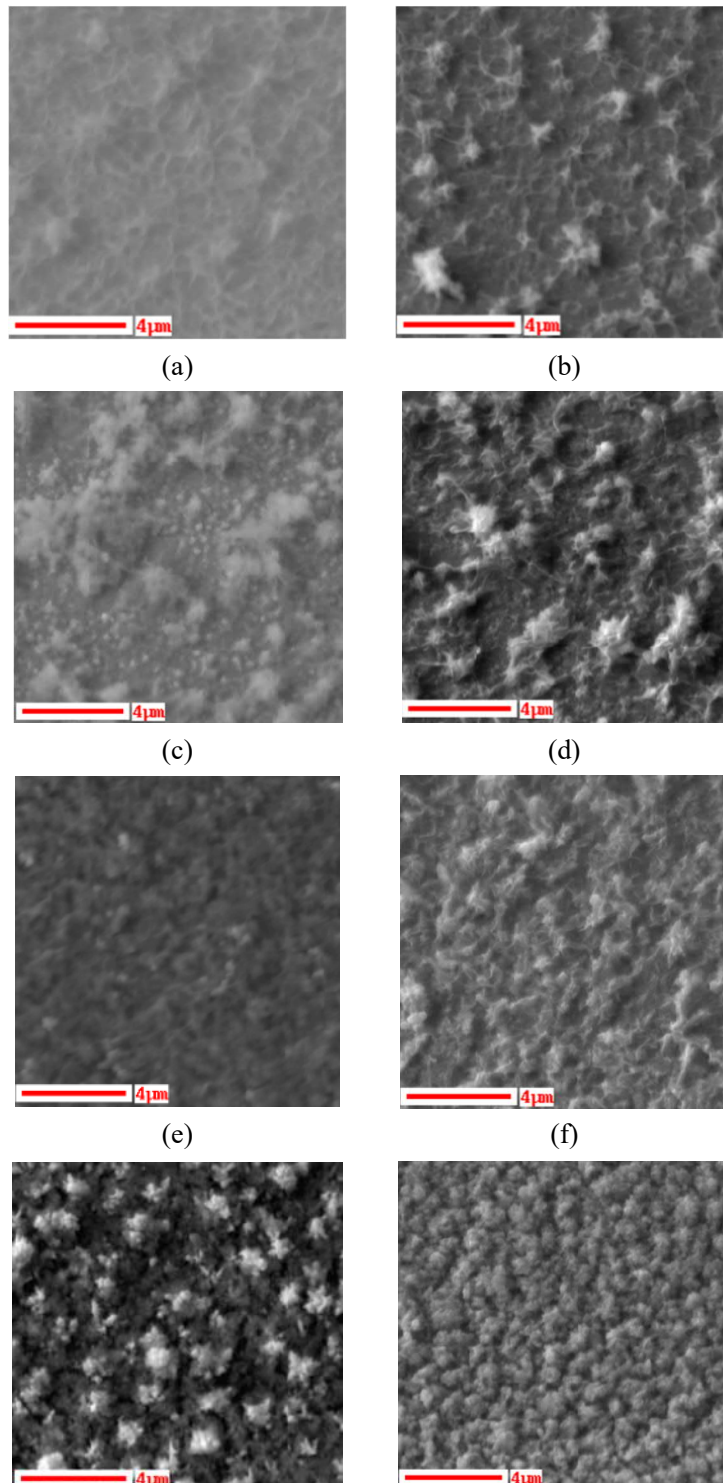
99 Fig.2 SEM image for the films deposited with different CuSO$_4$ concentrations (scale bar: 4 µm). (a): 0

100 mM, as-deposited, (b): 0 mM, annealed. (c): 1 mM, as-deposited, (d): 1 mM, annealed. (e): 2.5

101 mM, as-deposited, (f): 2.5 mM, annealed. (g): 10 mM, as-deposited, (h): 10mM, annealed.

102

103 Auger electron spectroscopy (AES) results are shown for the as-deposited films in Fig. 3(a) and for

104 the annealed films in Fig. 3(b). The surface of the films was Ar-etched for 15 to 30 s to remove

105 contaminants. All the thin films exhibited oxygen peaks around 500 eV and three iron peaks around

106 600-750 eV. In addition, as the concentration of CuSO$_4$ increased, three copper peaks around 800 –

107 900 eV were observed with larger intensity. A weak peak of sulfur around 150 eV was also detected

108 for the annealed film (Fig.3(b)), and it may be derived from the sulfate ion contained in the solution.

109 Sulfur could diffuse into the film from the residue of the solution on the surface during the annealing,

110 and then sulfur signal was observed in AES even after the Ar sputtering.

111 The composition ratios of thin films were calculated from the AES spectra using commercially

112 available standard chemicals Fe$_2$O$_3$ and CuO as the reference and are plotted as a function of CuSO$_4$

113 concentration in Fig.4. The ratios of Cu to Fe are shown in Table 1. As the CuSO$_4$ concentration

114 increased, the ratio of copper to iron increased almost linearly. After the annealing (Fig.4(b)), the

115 oxygen ratio decreased due to the dehydrating action. For the films without Cu, the compositions of

116 the as-deposited and annealed films almost correspond to those of FeOOH and Fe$_2$O$_3$, respectively.
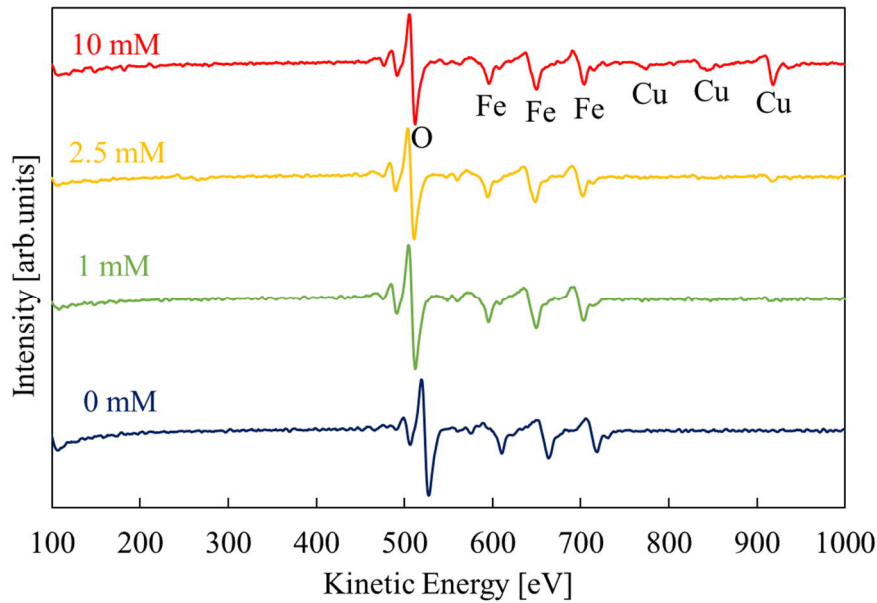
(a)
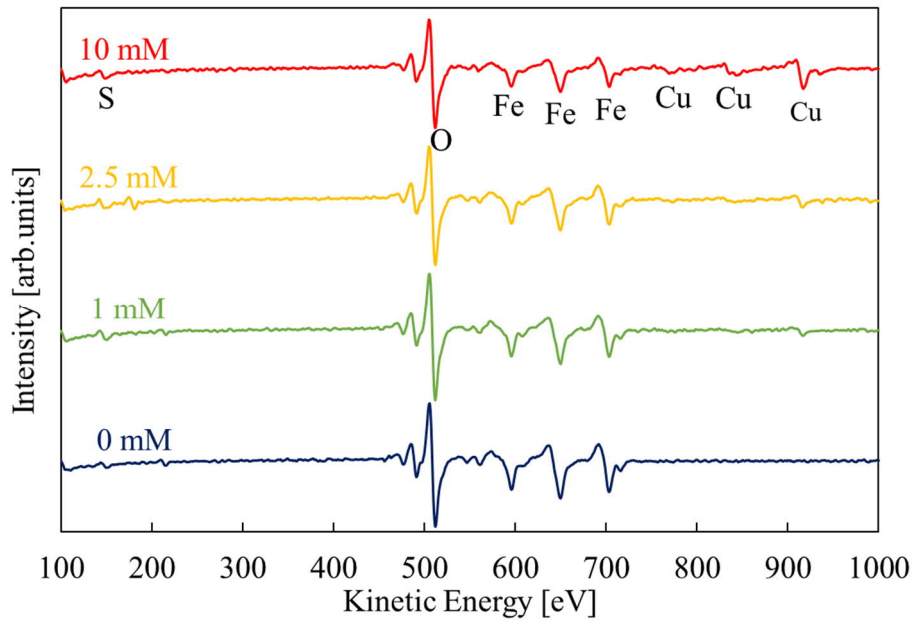
(b)

117   Fig.3   AES spectra for the selected (a) as-deposited and (b) annealed films deposited with different
118         $CuSO_4$ concentrations.
119

(a)

(b)
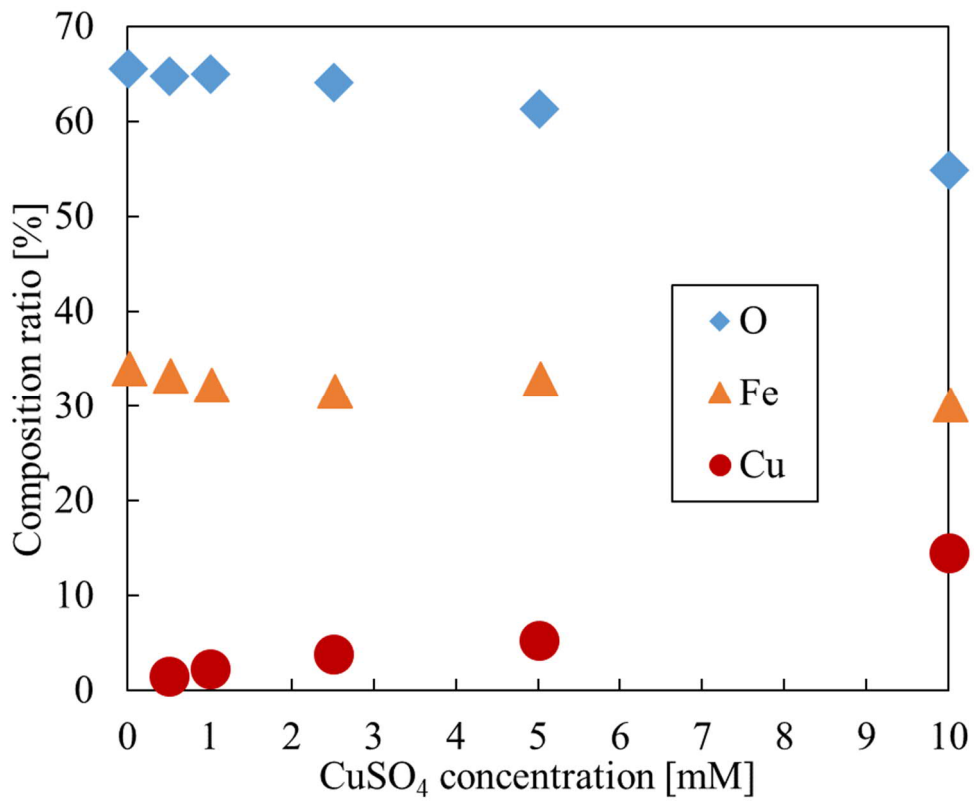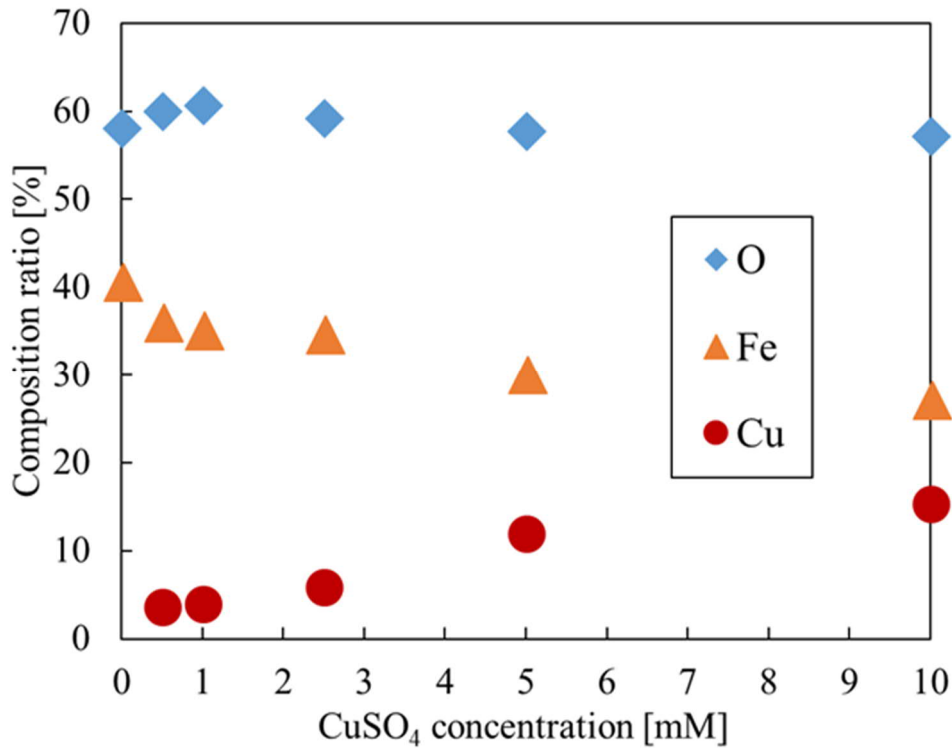
Fig.4   Compositional calculated from AES for the as-deposited (a) and annealed (b) films as a function of CuSO$_4$ concentration in the solution.

Table.1 Ratios of Cu to Fe in the films before and after the annealing for different CuSO$_4$ concentrations.

CuSO$_4$ [mM]	0.5	1	2.5	5	10
Cu/Fe (before annealing)	0.090	0.11	0.17	0.40	0.56
Cu/Fe (after annealing)	0.047	0.072	0.12	0.16	0.48

The XRD patterns measured for the as-deposited and annealed films are shown in Figs.5 (a) and (b), respectively. For the as-deposited film, most of the observed diffraction peaks are attributed to ITO, and therefore the films are considered to be amorphous. However, diffraction peaks were observed at 36.6º only or at 36.6º and 43.2º for the as-deposited films with CuSO$_4$ concentration of 2.5 mM or more, and these peaks are considered to be due to Cu$_2$O. Therefore, Cu$_2$O was also deposited with relatively large CuSO$_4$ concentration in the solution. After the annealing, a weak peak due to α-Fe$_2$O$_3$ was observed at 33º for the non-doped film. (According to the ICDD data in the figure, the peak at 33º is strongest among the peaks of α-Fe$_2$O$_3$, and the second strongest peak overlaps with the ITO peak.) In contrast, the α-Fe$_2$O$_3$ peak was not observed for the Cu-doped films. Thus, the Cu-doped films are considered to be amorphous even after the annealing. The Cu$_2$O peaks disappeared, and thus separated Cu$_2$O regions would be absent in the annealed film.

Figs.6 (a) and (b) represent the Raman spectra for the thin films before and after the annealing. The

138   Raman peaks are assigned on the basis of previous works for γ-FeOOH[4], Cu_2O[22], and Fe_2O_3 エラ

139   ー! 参照元が見つかりません。. For the thin films with $CuSO_4$ concentration of 0 to 1 mM, only the

140   γ-FeOOH peaks were observed near 252 and 384 cm^{-1}, and the peaks related to Cu-O were not

141   observed. For the thin film with $CuSO_4$ concentration of 2.5 mM, in addition to the γ-FeOOH peaks,

142   the Cu-O peaks were observed at 145, 517 and 628 cm^{-1}. On the other hand, for the thin films with

143      $CuSO_4$ concentration more than 5 mM, only Cu-O peaks were observed. After the annealing, all the

144   films exhibited strong iron oxide peaks, and the small peak due to Cu-O was observed under the

145   relatively Cu-rich condition ($CuSO_4$ concentration of 5 mM).
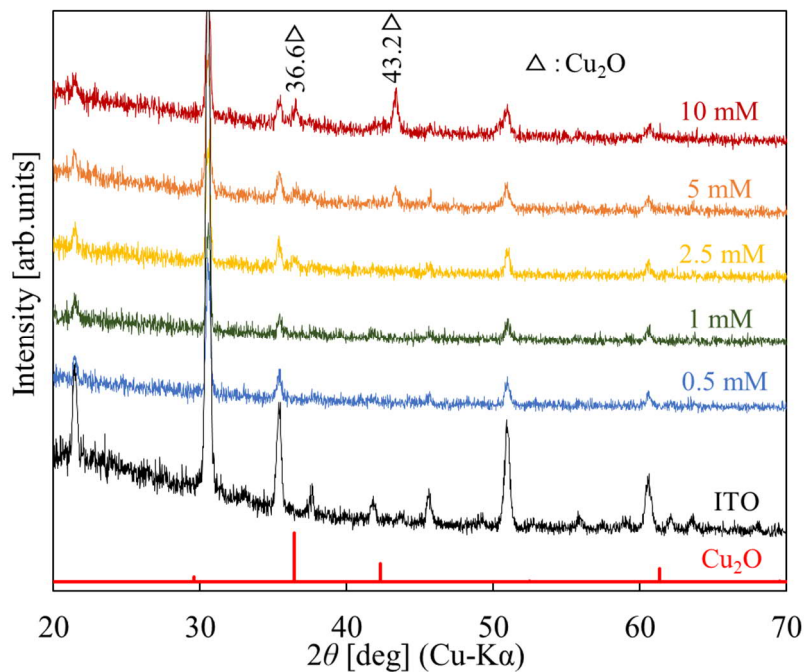
(a)
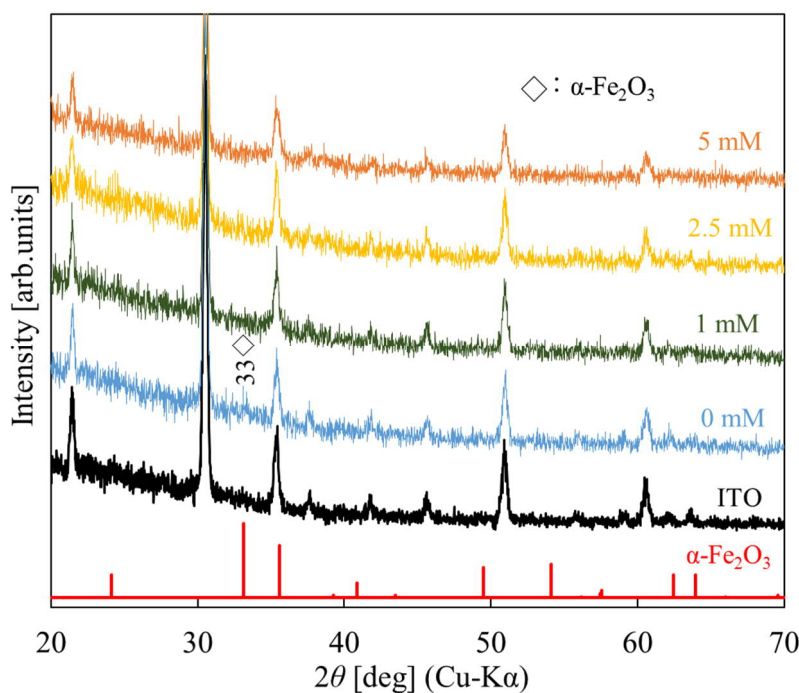
(b)

146   Fig.5   XRD patterns for the (a) as-deposited and (b) annealed films deposited with different $CuSO_4$

147   concentrations. ICDD data of Cu_2O and α-Fe_2O_3 are also plotted in Fig. (a) and (b), respectively.

148

(a)

(b)
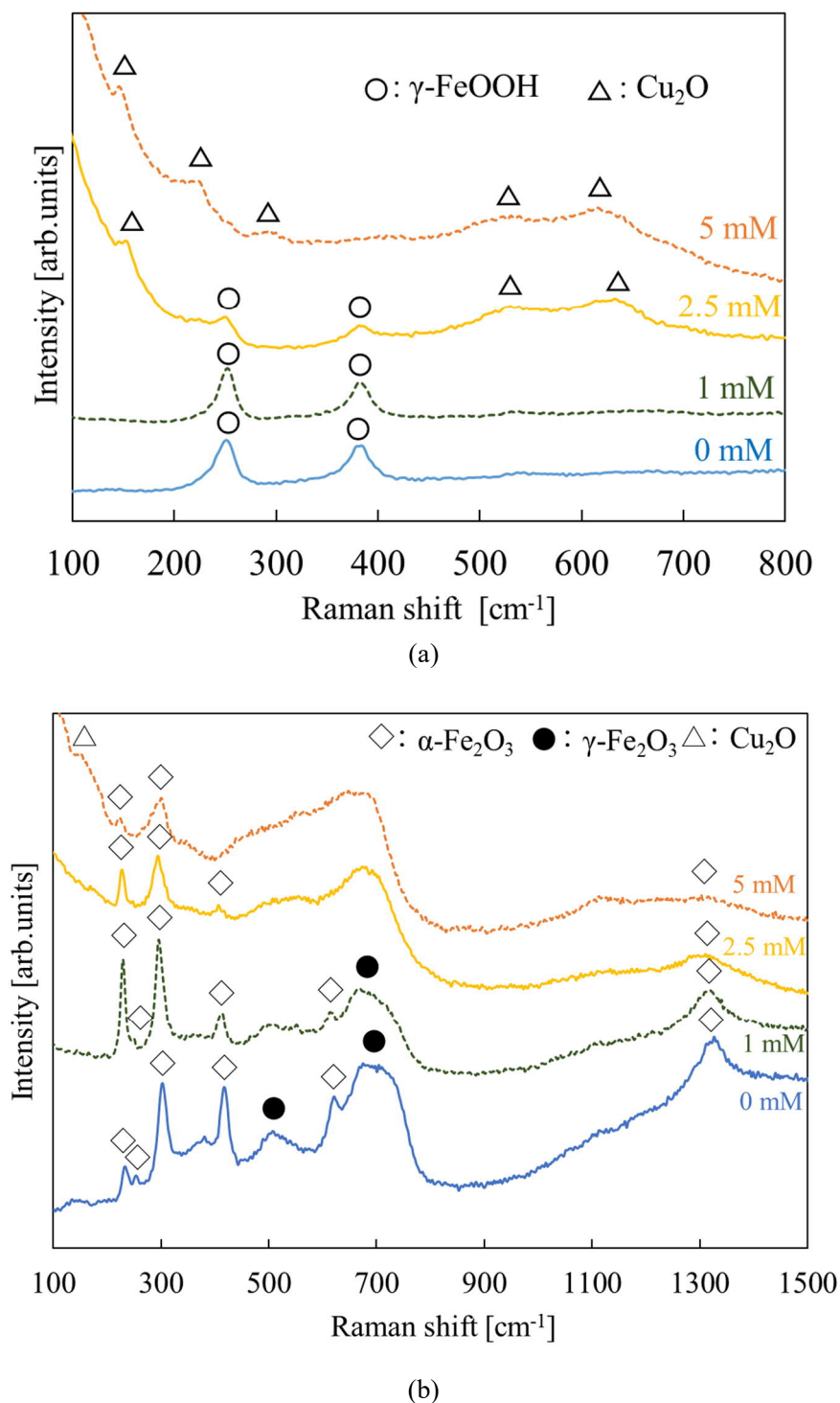
149   Fig.6   Raman spectra for the (a) as-deposited and (b) annealed films deposited with different $CuSO_4$

150   concentrations.

151

152   Figs.7 (a) and (b) illustrate the optical transmittance of the as-deposited and annealed films,

153   respectively. The absorption edge of the non-doped as-deposited γ-FeOOH film is observed around

154   560 nm, and thus the bandgap is estimated to be about 2.2 eV. As the concentration of $CuSO_4$ is

155   increased, the optical transmittance tends to decrease. In addition, with increasing $CuSO_4$

156   concentration, the transmission curve seems to shift to longer wavelengths, i.e., the bandgap of

157   Cu-doped iron oxide is smaller than 2.2 eV, although the bandgap cannot be evaluated accurately

158   because the absorption edge does not appear clearly. The transmission is significantly low for the films

159   deposited with 5 mM $CuSO_4$, and this could be because Cu_2O is included in the film, as revealed by

160   XRD. After the annealing, the bandgap was slightly decreased, and that of the non-doped film is about

161   2.1 eV. For the Cu-doped films, the transmission was increased in the long wavelength region (>700

162   nm) by the annealing.
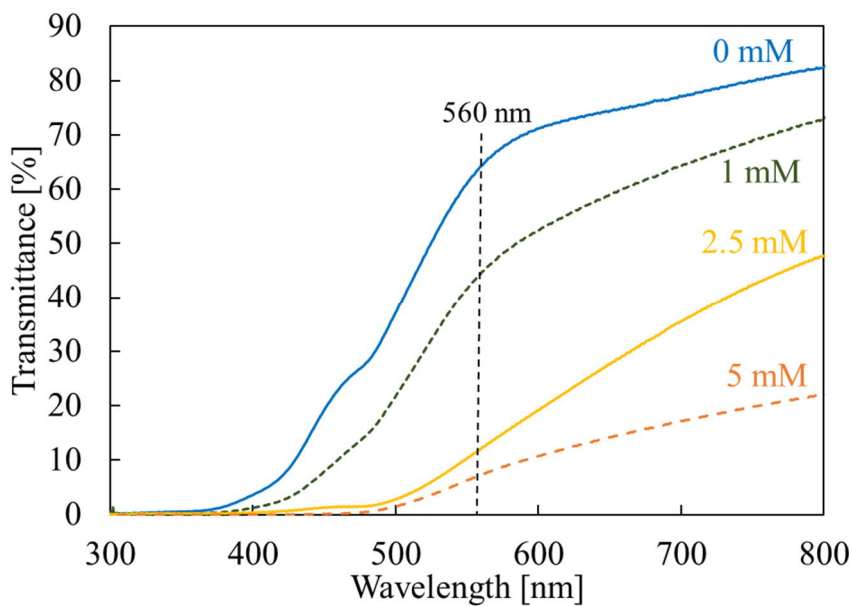
(a)
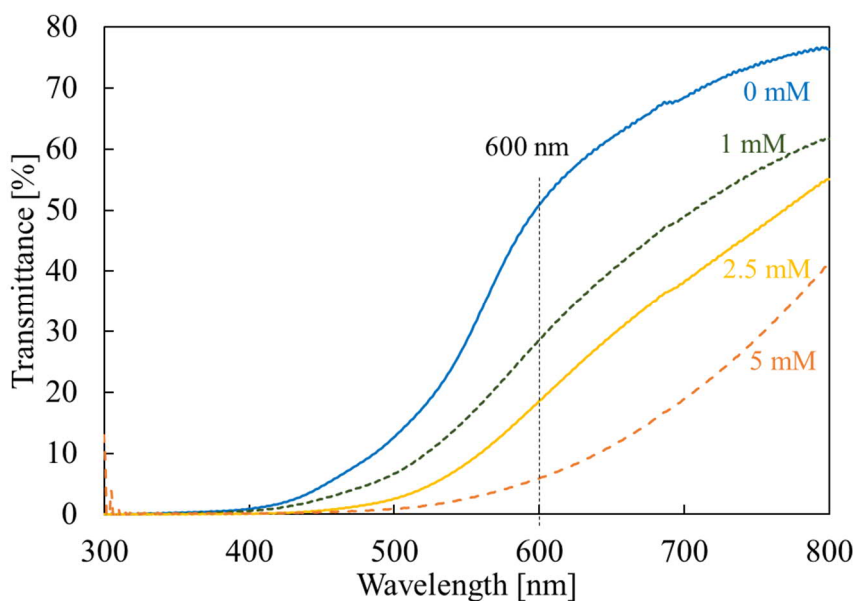
(b)

163   Fig.7   Optical transmittance of the (a) as-deposited and (b) annealed films deposited with different

164          $CuSO_4$ concentrations.

165

166   Figs.8 (a) and (b) show the photocurrent response in the PEC measurement for the as-deposited and

167 annealed films, respectively. For the non-doped film, only the positive photocurrent was observed,
168 which shows that the film is n-type. The negative photocurrent response, characteristics of p-type
169 semiconductor, was observed for the films deposited with $CuSO_4$ concentration of 1 mM or more.
170 However, n-type photocurrent response was also confirmed, and thus the conduction type would be
171 close to intrinsic. After the annealing, only the negative photocurrent response was observed for the
172 Cu-doped films, thus we can conclude that those Cu-doped films are p-type. As noted in the
173 introduction, annealing in air (oxidizing ambient) would reduce the donor defects due to oxygen
174 deficiency. Thus, the p-type character was enhanced by the annealing. For the film deposited with
175 $CuSO_4$ concentration of 0.5 mM, p-type photocurrent was not observed clearly. Thus, considering the
176 elemental composition shown in Fig.4, one may consider that Cu-doped iron oxide is converted to
177 p-type when Cu/Fe ratio is larger than about 0.1. With increasing $CuSO_4$ concentration, the p-type
178 negative photocurrent tends to increase.

179   Fig.9 shows the Mott-Schottky plot of the capacitance by the electrochemical impedance
180 measurement for the as-deposited and the annealed films deposited with 0 and 5 mM $CuSO_4$. For the
181 non-doped samples, a positive slope was observed both before and after the annealing, and the
182 flat-band potential would be in the negative range. Thus they showed typical n-type behaviors. On the
183 other hand, the annealed sample deposited with 5 mM $CuSO_4$ had a positive slope, and thus it was
184 found to be p-type. The as-deposited sample with 5 mM $CuSO_4$ did not show clear n-type or p-type
185 behavior. This seems consistent with the PEC results that the p-type character was enhanced by the
186 annealing.

187

(a)

(b)
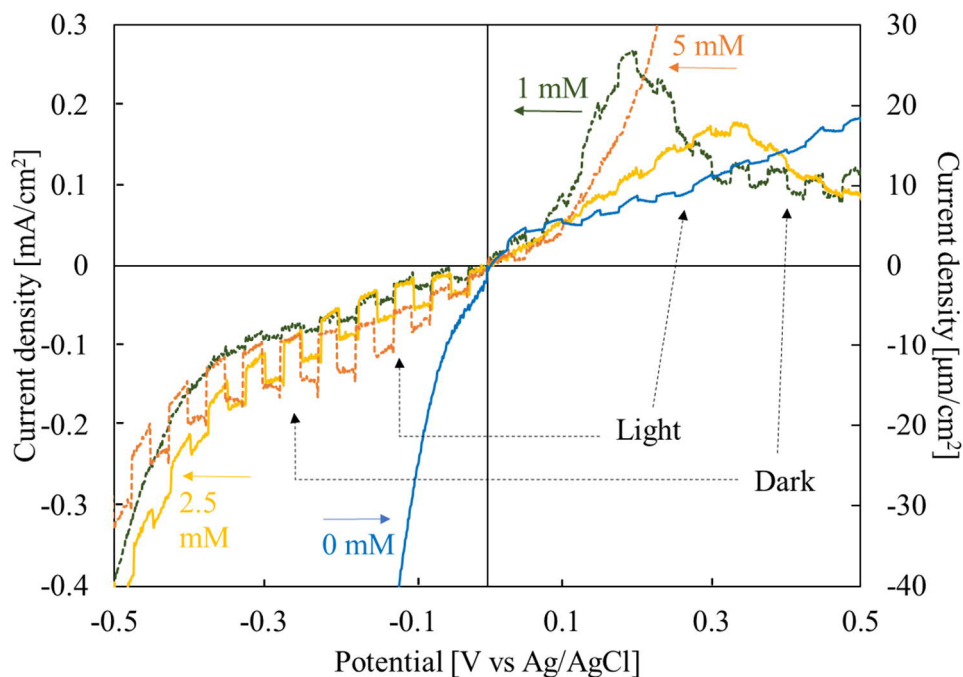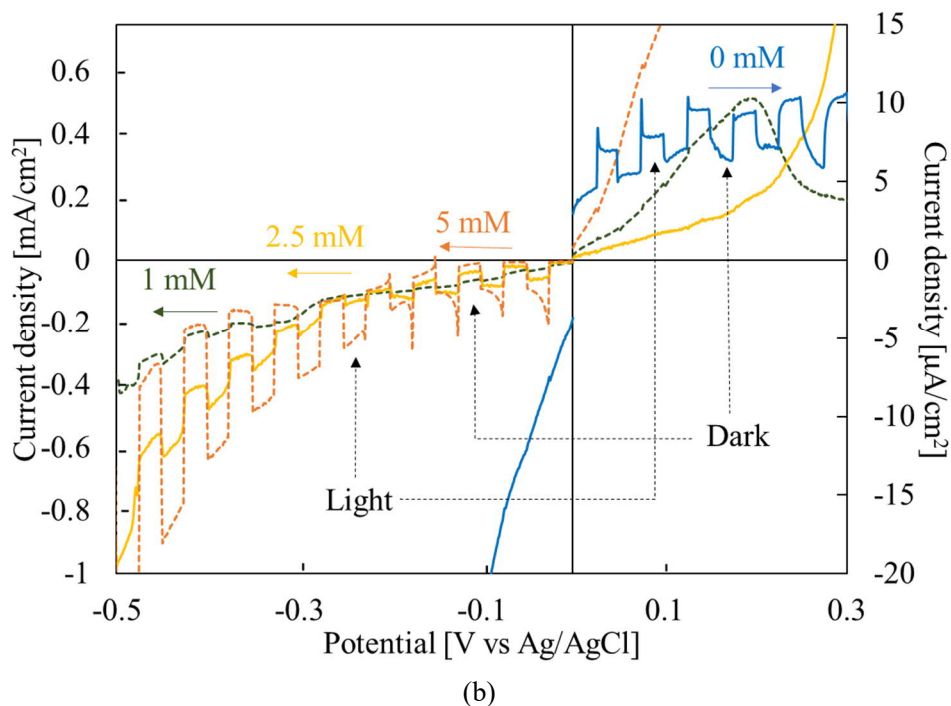
188 Fig.8 Photocurrent responses in the PEC measurement for the (a) as-deposited and (b) annealed films
189   deposited with different CuSO₄ concentrations.

190
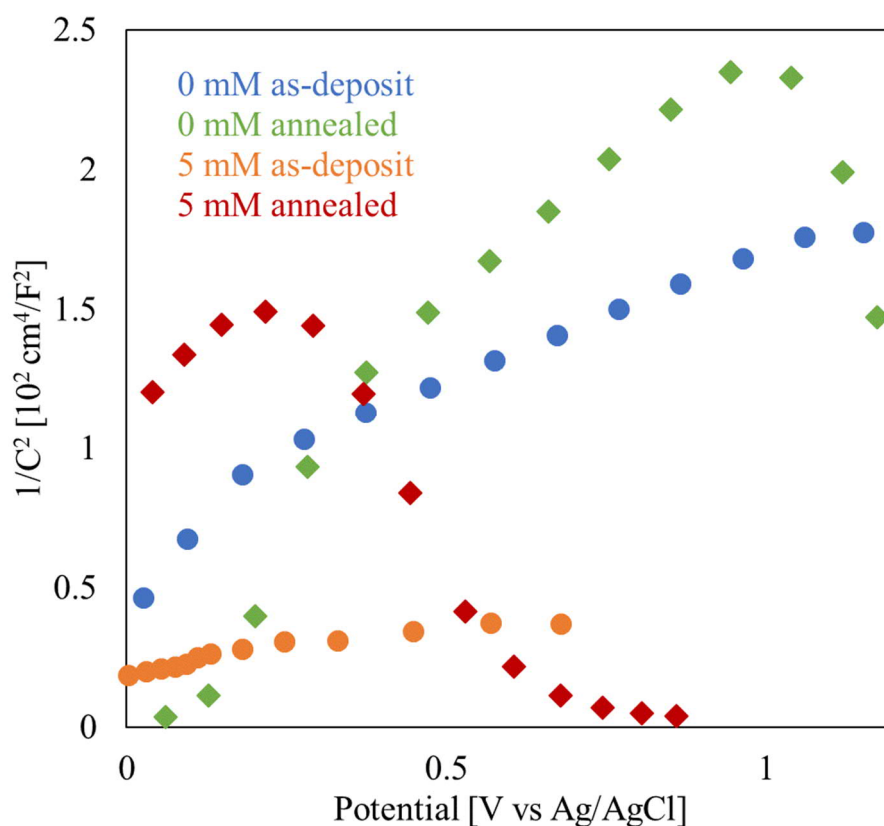
191

192 Fig.9 Mott-Schottky plot for the as-deposited and the annealed films with 0 and 5 mM CuSO₄
193   concentrations.

194

195 As noted above, the annealed Cu-doped films exhibited only the negative, p-type photo-response in

the PEC measurement. If the doped Cu atoms were not distributed uniformly but formed separated Cu_2O regions in the n-type Fe_2O_3 matrix, then the positive (n-type) photocurrent would also be observed. Therefore, the PEC results indicate absence of such separation for the annealed films. In XRD, the peaks due to Cu_2O were observed for $CuSO_4$ concentration of 2.5 mM or more before the annealing, but those peaks were not observed after the annealing. This also indicates that separate Cu_2O phase is not included in the annealed films. On the basis of all the results given above, we can conclude that the films deposited with $CuSO_4$ concentration of 2.5 mM or more and annealed in air will be suitable for photovoltaic and photoelectrode applications, because those films have clear p-type conductivity and photosensitivity.

4. Summary

Cu-doped iron oxide films were deposited by ECD from an aqueous solution containing 50 mM $FeSO_4$ and 0-10 mM $CuSO_4$. Without Cu doping, the deposit was γ-FeOOH, having the band gap of about 2.2 eV and n-type conductivity. For the films deposited with $CuSO_4$ concentrations of 1 mM or more, p-type photoresponse was confirmed in the PEC measurement. The annealing in air improved integrity of the films and enhanced p-type character. The bandgap of the Cu-doped films was slightly smaller than that of non-doped iron oxide.

Acknowledgements

References

[1] Sivula K, Formal F L and Gratel M 2011 *Chem. Sus. Chem.* **4** 432-449

[2] H. Li, W. Li, Y. Zhang, T. Wang, B. Wang, W. Xu, L. Jiang, W. Song, C. Shu, and C. Wang 2011 *J. Mater. Chem*, **21** 787

[3] Y. Jia, T. Luo, X.-Y. Yu, Z. Jin, B. Sun, J.-H. Liu, and X.-J. Huang, *New J. Chem.* **37**, (2013), 2551-1556

[4] J. J. M. Vequizo, M. Ichimura 2013 *Appl. Phys. Express* **6** 125501

[5] E. E. Carpenter, V. Cestone, G. Landry, V. G. Harris and K. M. Kemner 2003 *Chem. Mater.* **15** 1235-1236

[6] M. Schneider and M. Stratman 1992 *Ber. Bunsenges. Phys. Chem.* **96** 1731-1736

[7] J. Majzlan, L. Mazeina and A. Navrotsky 2007 *Geochim. Cosmochim. Acta.* **71** 615-623

[8] T. Ishikawa, H. Nishimori, I. Abe, and K. Kandori 1993 *J. Mater. Sci. Lett.* **12** 1359-1361

[9] U. Schwertmann and R.M. Corneil 1991 *Iron Oxides in the Laboratory,* VCH Publishers*,* New York, 93-99

[10] T. Nakanishi, Y. Masuda, and K. Koumoto 2005 *J. Crystal Growth* **284** 176-183

[11] H. Antony, S. Peulon, L. Legrand, and A. Chausse 2004 *Electrochim. Acta.* 50 1015-1021

[12] L. Martinez, D. Martin, M. Gabas, J. R. Ramos-Barrado, E. Quagliata and E. A. Dalchiele 2007 *J. Electrochem. Soc.* **154** 3 D126-D133

236   [13] H. Naono and K. Nakai 1989 *J. Colloid Interface Sci.* **128** 146-156

237   [14] W. B. Ingler Jr. and S. U. M. Khan 2005 *Int. J. Hydrogen Energy* **30** 821-827

238   [15] W. B. Ingler Jr, P. J. Baltrus and S. U. M. Khan 2004 *J. Am. Chem. Soc.* **126** 10238-10239

239   [16] C. Leygraf, M. Hendewerk and G. Somorjai 1983 *J. Solid. State. Chem.* **48** 357-367

240   [17] Y. Lin, Y. Xu, M. T. Mayar, Z. I. Simpson, G. McMahon, S. Zhou, D. Wang 2012 *J. Am. Chem.*
241   *Soc.* **134** 5508-5511

242   [18] G. H. A. Therese and P. V. Kamath 2000 *Chem. Master* **12** 1195

243   [19] H. Matsui and H. Tabata 2006 *J. Surf. Sci. Soc. Japan* **27** 708

244   [20] K. Nakaoka, J. Ueyama and K. Ogura 2004 *J. Electrochem. Soc.* **151** C661-C665

245   [21] Y. Song and M. Ichimura 2012 *Jpn. J. Appl. Phys.* **51** 10NC39

246   [22] Y. Liu et al. 2015 *Appl. Phys. Lett.* **106** 123901

247   [23] D. L. A. de Faria, S. V. Silva and M. T. de Oliveira 1997 *J. Raman Spectrosc*, **28** 873-878

248